PHYSICAL REVIEW B VOLUME 18, NUMBER 3 1 AUGUST 1978

New aspects of axial-to-planar channeling transition in a noncubic compound crystal, α-Al_2O_3

A. Carnera, G. Della Mea, A. V. Drigo, S. Lo Russo, and P. Mazzoldi
Istituto di Fisica dell'Università, Unità Gruppo Nazionale di Struttura della Materia del Consiglio Nazionale delle Ricerche, Via Marzolo 8, 35100 Padova, Italy

G. G. Bentini, A. Desalvo,* and R. Rosa
LAMEL, Consiglio Nazionale delle Ricerche, Via Castagnoli, 1, 40126 Bologna, Italy
(Received 27 January 1978)

The axial-to-planar channeling transition in α-Al_2O_3 has been studied both experimentally and by computer simulation for various axes and planes. Particular interest has been turned to the $\langle 0001\rangle \rightarrow \{1\bar{2}10\}$ transition, characterized by a shoulder, for the O sublattice, much higher than 100%. Both experiments and calculations, the latter carried out also varying the lattice arrangement, show that these shoulders are determined by the mutual flux peaking due to the two sublattices. In particular, calculations show that the relative spacing between the two sublattices in the real crystal is such as to maximize the effect. Computed trajectories are in agreement with the model of resonance dechanneling by Kumakhov and Wedell.

I. INTRODUCTION

When a collimated beam of energetic ions undergoes the axial-to-planar channeling transition, a maximum occurs in the stopping power of the channeled particles and the dechanneled fraction,[1,2] in Rutherford backscattering,[3] nuclear reactions,[4] and x-ray[5] yields, while minima occur in the transmitted intensity.[6,7]

Computer simulations showed that the transition is associated with an instability of the planar trajectory depending on the nonconservation of transverse energy, owing to the discrete structure of the lattice planes.[8] Some authors suggested that the shoulders are caused by a resonance in the trajectory oscillations between two adjacent atomic planes, which occurs when the corresponding wavelength in the plane normal to the axial channel is comparable to the separation of rows inside the planar channel.[7,9]

Some results in the case of a solid solution TiO_x containing a relatively weak impurity sublattice showed that at the axial-to-planar channeling transition to a mixed plane the channeled ion can distinguish between stronger and weaker rows and penetrates preferentially near the latter ones, giving rise to much higher shoulders at the impurity than at the matrix site.[10,11]

In the experiments concerning monoatomic crystals or TiO_x solid solutions the transition shoulders turn out to be always lower than the 100% random level. On the contrary, preliminary results on α-Al_2O_3 diatomic crystals, formed by sublattices of comparable strength, showed axial-to-planar transitions characterized by much higher than 100% shoulders.[12] In the present paper we have extended the experimental investigations to different transitions from various axes to various planes. The results have been also analyzed by computer calculations, obtaining a satisfactory interpretation of the most significant experimental observations.

II. EXPERIMENTAL PROCEDURE

A detailed account of the experimental technique and of the procedure for data analysis has been reported previously.[13,14] Therefore only a short description will be given here.

The α-Al_2O_3 single crystals, obtained from Materials Research Corporation, were in the form of optically polished disks, cleaned in a solution of boiling sulfuric acid for about 1 hour and subsequently annealed in vacuum at high temperature.

The incident 1.6-MeV He^+-ion beam, obtained from the 2.0-MeV Van de Graaff accelerator of Laboratori Nazionali di Legnaro, was collimated to better than 0.03°. The beam current was kept at a value of the order of 1 nA to reduce pile-up effects and too high counting rates. The damage induced by the analyzing beam was avoided by translating the beam parallel to itself in order to change the analyzed region of the sample during the angular-dip measurements.[13]

III. α-Al_2O_3 STRUCTURE

The structure of α-Al_2O_3 is corundum and can be visualized as an approximately hexagonal-close-packed lattice of oxygen atoms with the small aluminum atoms occupying two thirds of the octahedral interstitial sites between the oxygen layers. However, the oxygen atoms are slightly displaced from the hcp lattice sites.

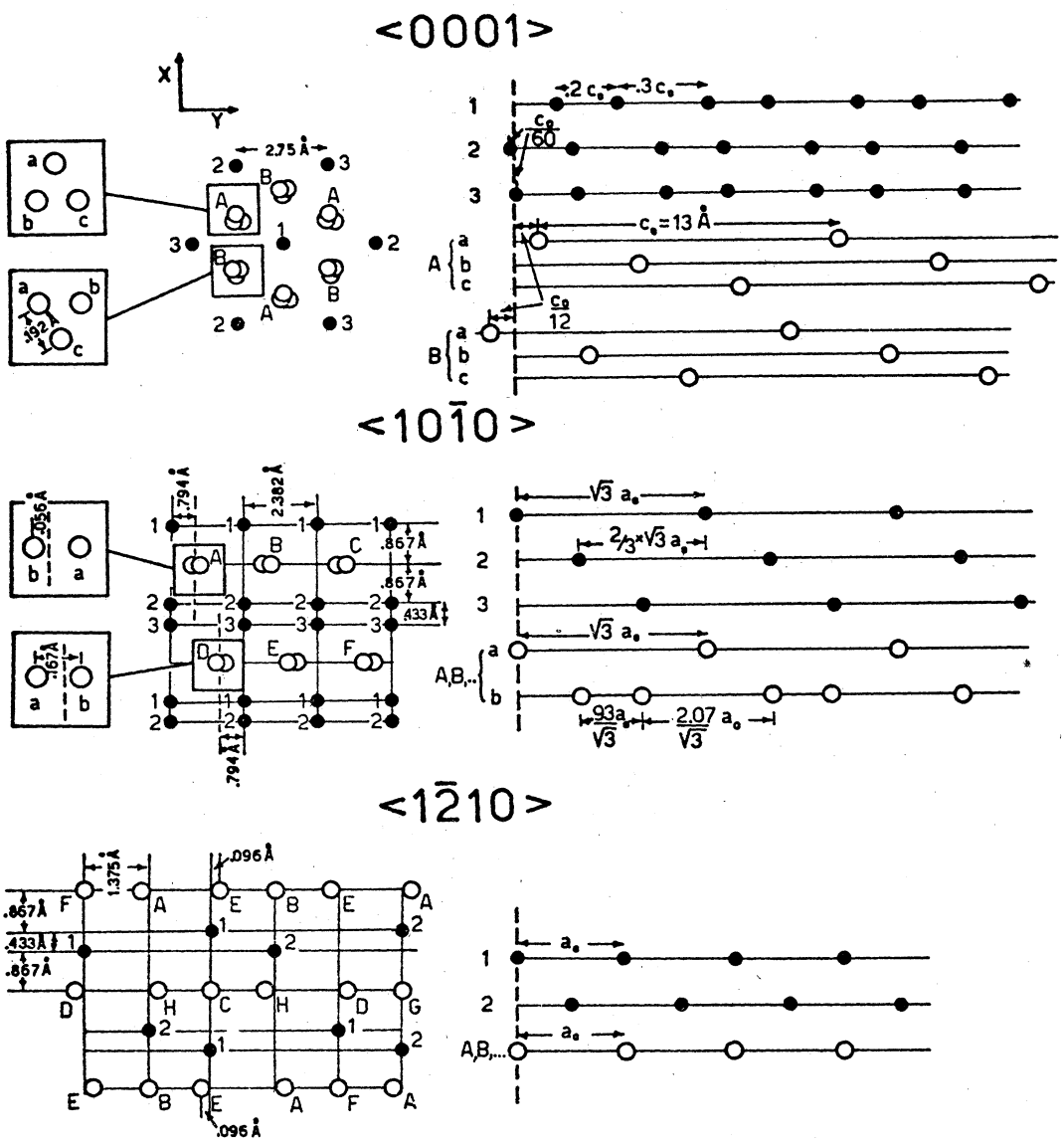

FIG. 1. Atomic arrangements for ⟨0001⟩, ⟨10$\bar{1}$0⟩, and ⟨1$\bar{2}$10⟩ axial directions in α-Al_2O_3. Full and open circles refer to Al and O atoms, respectively. The arrangements shown on the left are endviews of the channels. Numbers and letters refer to the individual strings shown on the right. As for the ⟨10$\bar{1}$0⟩ and ⟨1$\bar{2}$10⟩ directions all the oxygen rows have the same atom sequence, respectively, shown. However the starting atom rows labelled with different letters have different shifts with respect to the perpendicular plane indicated by the dashed line. The X and Y directions shown for the ⟨0001⟩ channel refer to the tilt directions of the computer model.

Figure 1 gives the atomic arrangement for the ⟨0001⟩, ⟨1$\bar{2}$10⟩, and ⟨10$\bar{1}$0⟩ axial directions. The aluminum sites are denoted by a full circle and the oxygen sites by an open one. The enlarged insert displays the displacement of the oxygen atoms from the hcp lattice sites. With regard to the ⟨0001⟩ axis, in the following the X direction is taken parallel to the {10$\bar{1}$0} plane and the Y direction parallel to the {1$\bar{2}$10} plane.

Figure 2 shows the atomic-layer sequence for the main planes. The {0001} plane corresponds to the Y direction, both for the ⟨10$\bar{1}$0⟩ and ⟨1$\bar{2}$10⟩ axes.

IV. COMPUTER MODEL

The computer model is the same one used by us in a previous paper.[11] Alternating layers of Al and O atoms, all shown projected onto the {0001} plane

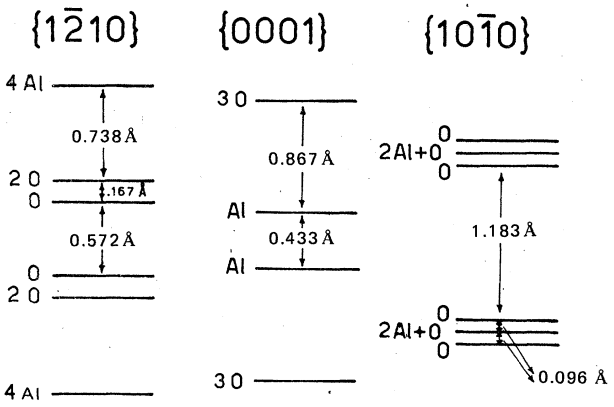

FIG. 2. Planar atomic arrangement and interplanar spacings in α-Al_2O_3.

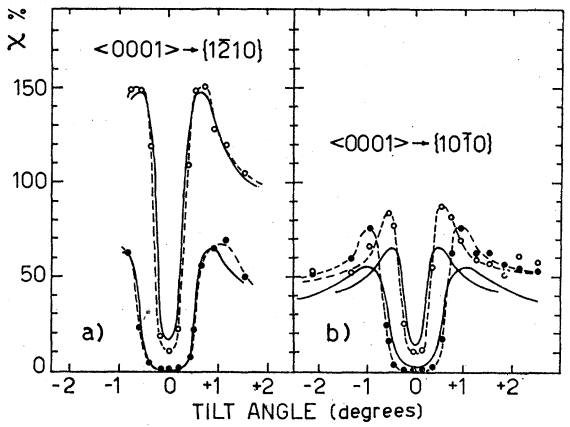

FIG. 3. Experimental and computed yields for the ⟨0001⟩ to {1$\bar{2}$10} and to {10$\bar{1}$0} channeling transitions in α-Al_2O_3. Probe: 1.6-MeV He^+ ions. Full and open circles refer to the experimental yields from the Al and O atoms, respectively. Full lines are the results of the computer simulations.

in Fig. 1, follow in our model at a distance of $c_0/12 = 1.08$ Å. This introduces a slight simplification compared with the real structure because Al atoms lying $\frac{1}{60}c_0 = 0.22$ Å both below and above are made to coincide in a unique plane. No other projection onto a unique layer of different Al and O sheets was made because the results turned out to be very sensitive to this further simplification.

The flux was averaged over 500 Å of penetration, a value comparable with the resolution of the experimental apparatus and sufficient to eliminate fluctuations and depth oscillations. Due to the low depth, stopping power and electronic scattering were neglected. The assumed Debye temperature was 950 °K as in Ref. 13. The flux was measured over a square grid of the order of the Thomas-Fermi screening radius. To improve statistics the flux was reduced in $\frac{1}{4}$ of the hexagonal cell: in the axial case $\frac{1}{12}$ of the cell is sufficient, but in the planar case such a high symmetry is not maintained. Due to the somewhat complex arrangement of the oxygen atoms, when projected onto the basal plane, a square grid does not cover exactly the area corresponding to a circle of radius a_{TF} around the oxygen atoms. Therefore, the computed values are affected by a certain error, at the most of the order of 10%.

Calculations were performed with the CYBER 72/76 CDC System of the "Centro di Calcolo Elettronico dell'Italia Nord-Orientale." The computation time for each trajectory was 0.36 sec; 500 histories were usually sufficient.

V. RESULTS AND DISCUSSION

A. Comparison with experiments

Figure 3 shows both experiments and calculations for the transition from the ⟨0001⟩ axis to the {10$\bar{1}$0} plane [left-hand side, (a)] and to the {1$\bar{2}$10} plane [right-hand side, (b)], respectively. Computer calculations follow fairly well the experimental curves.

In the case of the ⟨0001⟩→{10$\bar{1}$0} transition the calculated shoulders lie somewhat lower than the experimental ones but the minimum yield and the half width are well reproduced. This transition resembles the one previously observed by us in the TiO_x system [see Figs. 5(c) and 5(d) of Ref. 10 or Figs. 10(c) and 10(d) of Ref. 11].

On the contrary the ⟨0001⟩→{1$\bar{2}$10} transition shows new interesting features, i.e., very high shoulders for the oxygen sublattice, of the order of 150%. This value must be compared with a planar asymptotic value of 75%. The observed shoulders appear to be very high compared with the computer results obtained by Barrett in a simple Al lattice, which predict much lower shoulders, of the order of (110–120)% for planes having $\chi = (80–90)\%$.[15] Similar results were obtained by Ryabov in W,[16] and by Hellborg in mixed planes of CaF_2.[17]

Figure 4 shows the flux map for both axial-to-planar channeling transitions, ⟨0001⟩→{10$\bar{1}$0} and ⟨0001⟩→{1$\bar{2}$10}. The intermediate cases shown are at 0.8° from the axis, which correspond to the maximum yield for both oxygen and aluminum in Al_2O_3. The transition displayed in the lower side is similar to the one shown in our paper on TiO_x, in which at the transition the planar flux breaks mostly at the weaker row.[11]

The upper side, referring to the other transition, shows new interesting features. By comparing the

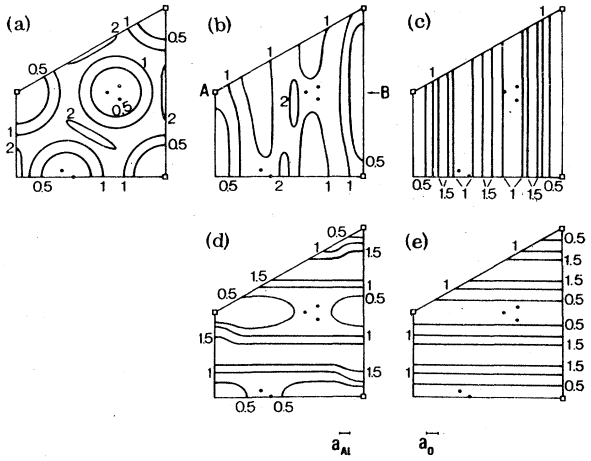

FIG. 4. Flux-contour plot of 1.6 MeV He^+ along the $\langle 0001 \rangle$ axis in α-Al_2O_3 for different tilt angles θ. The map is limited to $\frac{1}{4}$ of the hexagon of Fig. 1. a_{Al} and a_O, the Thomas-Fermi radii relative to the two atoms, are shown for comparison on the same scale. (a) $\Theta_x = \Theta_y = 0$; (b) $\Theta_x = 0°$, $\Theta_y = 0.8°$; (c) $\Theta_x = 0°$, $\Theta_y = 7°$; (d) $\Theta_x = 0.8°$, $\Theta_y = 0^0$; (e) $\Theta_x = 7°$, $\Theta_y = 0^0$.

contour curve corresponding to a flux of two times the random flux near the O atoms in Fig. 4(b) with the flux in the planar case [Fig. 4(c)], one sees that this contour curve is essentially due to a rearrangement of the 1.5 flux curve lying between the O planes.

B. Computer experiments

1. Isolated O and Al sublattices

To better understand the latter feature we made some computer experiments. As Morgan and Jackson point out[18] "One of the powerful advantages of computer simulation is the ability to study ···hypothetical situations for lattices and situations which do not exist in nature. In this way one can isolate the roles of various effects by deliberately constructing lattices in which they are likely to show up strongly." Figure 5 shows the computed flux on Al and O sites both in Al_2O_3 (curves *c* and *d*) as shown before [see continuous lines of Fig. 3(a)] and in the isolated Al (curve *a*) and O sublattices (curve *b*). The figure shows that the Al sublattice contributes to increase the O shoulder up to 150%, but also that this shoulder is already high (~105%) when only the O sublattice is present. To display better the contribution of both sublattices to flux peaking, in Fig. 6 we plotted the flux distribution along the *A-B* line of Fig. 4(b). Continuous, dashed and dot-dash curves refer to Al_2O_3, oxygen, and aluminum sublattices, respectively. The left-hand side of

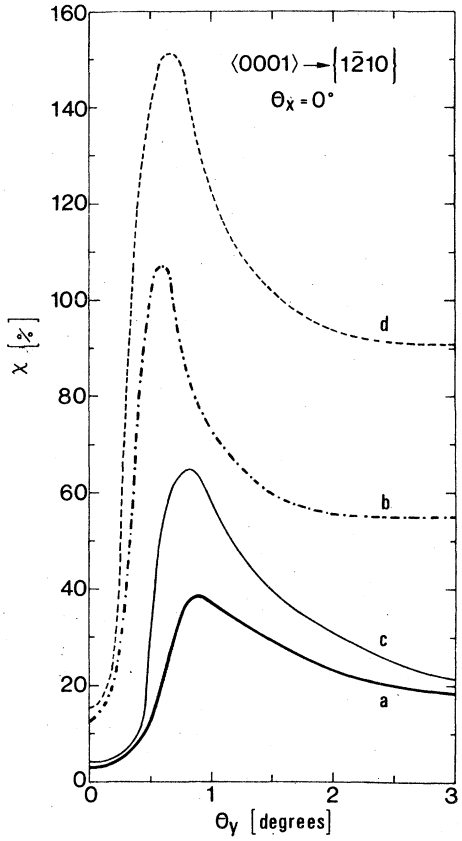

FIG. 5. Computed yield for the $\langle 0001 \rangle$ to $\{12\bar{1}0\}$ channeling transition in α-Al_2O_3. Curves *c* and *d* refer to the computed yields at Al and O sites in Al_2O_3, respectively, as already shown in Fig. 3 (a). Curve *a* refers to the computed yield at the Al site with the O sublattice "switched off," and curve *b* to the computed yield at the O site with the Al sublattice "switched off."

Fig. 6 shows the flux distribution for the planar case (which of course is independent from the position of *A-B*) both for Al_2O_3 [see Fig. 4(c)] and for the two separate sublattices. The important point to remark is that the O sublattice is strong enough to produce flux peaking between O planes. The Al sublattice enhances both this flux and the flux at the O planes. The right-hand side of Fig. 6 shows the flux distribution along *A-B* at the transition. Note that the O_1 and O_2 arrows denote atoms lying far apart from the *A-B* line and the O_4 arrow denotes atoms which lie slightly above and below *A-B*.

One sees that the high flux at O atoms at the transition is attributable to two reasons. The first one is the effect of the Al sublattice which pushes the flux between the Al and O planes on the O atoms [see the peak on the right on the continuous curve of Fig. 6(b)]. But even without the Al sublattice, at

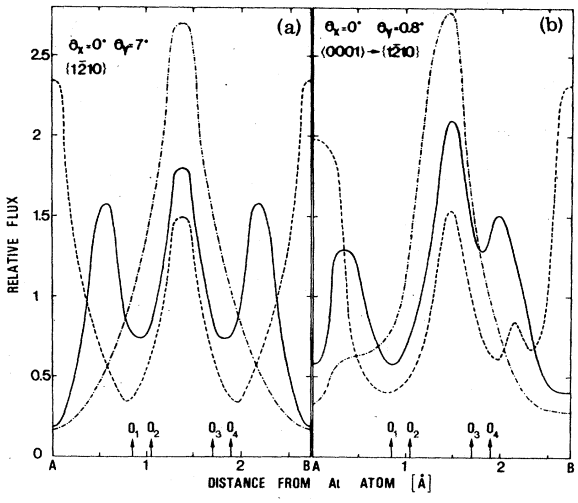

FIG. 6. Computed flux along the A–B line of Fig. 4(b). Continuous, dashed and dot-dash line refer to Al_2O_3, O sublattice alone, and Al sublattice alone respectively. Left-hand side (a) refers to $\{1\bar{2}10\}$ planar channeling, right-hand side (b) to $\Theta_y = 0.8°$, corresponding to the shoulder for the $\langle 0001\rangle \rightarrow \{1\bar{2}10\}$ transition. O_1, O_2, O_3, and O_4 refer to the oxygen-plane position. As shown in Fig. 4, O_1 and O_2 correspond to oxygen atoms lying well below the A–B line, O_3 lies on A–B, and O_4 corresponds to two atoms lying slightly below and above A–B.

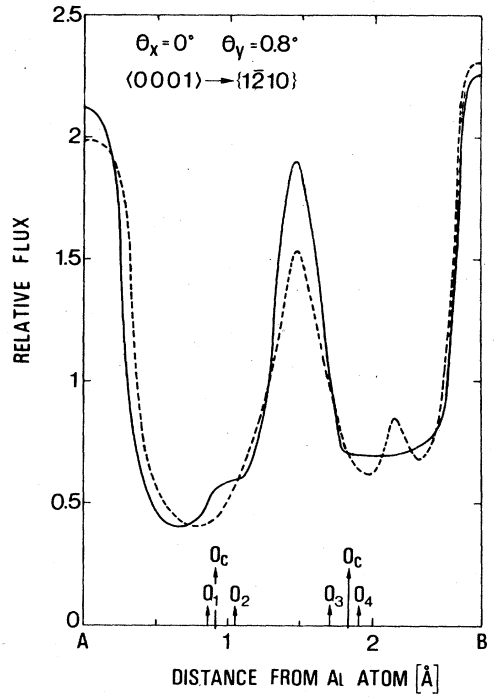

FIG. 7. Computed flux as in Fig. 6(b), only for the O sublattice. The continuous line refers to a fictitious O sublattice in which all the O atoms lie exactly in an hcp arrangement. The dashed line is shown for comparison and is the same as in Fig. 6(b). O_1, O_2, O_3, and O_4 have the same meaning as in Fig. 6, while O_c denotes the position of the oxygen planes in the fictitious structure (note that only the O_c lying between O_3 and O_4 lies on A–B).

the transition a high flux on the O atoms occurs owing to the shift of the flux between the two O planes towards the O atoms.

2. *Effect of O-atom displacements*

As mentioned in Sec. V A., shoulders of the order of unity for a plane with a low minimum yield, as observed in the isolated O sublattice, appear to be a new feature deserving further investigation. To clarify the origin of this, we modified the O sublattice by arranging the O atoms exactly on an hcp lattice. This is obtained by making the three O atoms lying on the vertices of the small equilateral triangle (see Fig. 1) collapse on a unique row at the center. Figure 7 compares the results at the transition [continuous line, the dashed line is the same as in Fig. 6(b)], O_c denoting the new position of the O atoms. The only effect of this displacement is just to eliminate the fluctuation around the O atoms, leaving the average flux unchanged. Note that, while the small peak of Fig. 6(b) at about 2 Å from the A position in the O sublattice (dashed line) is due to the fine structure of the oxygen row, the peak at about the same position in the Al_2O_3 lattice (continuous line) is of completely different origin, as mentioned above when discussing Fig. 6(b).

3. *Interplanar-spacing influence*

The experimental results reported in Fig. 8, referring to the axial-to-planar $\langle 10\bar{1}0\rangle \rightarrow \{1\bar{2}10\}$ and $\langle 1\bar{2}10\rangle \rightarrow \{0001\}$ transitions, indicate a higher than 100% yield shoulder for the oxygen and aluminum atomic sites, respectively. As shown in Fig. 2 the $\{1\bar{2}10\}$ planes are characterized by two closer oxygen planes, while the situation is reversed (two closer aluminum planes) in the $\{0001\}$ case. This suggests an effect on the yield shoulders of the spacing between nearest planes.

Computer experiments were carried out to see the effect of varying the interplanar spacing between the two nearest $\{1\bar{2}10\}$ O planes, leaving unaltered the dimension of the unit cell show in Fig. 1. Figure 9 shows the spacing for the computed cases. The dashed lines correspond to the position of the center of mass of the O atoms and in the following we refer only to its coordinates with respect to the Al planes for simplicity's sake. Note that the distance between Al planes corresponds to

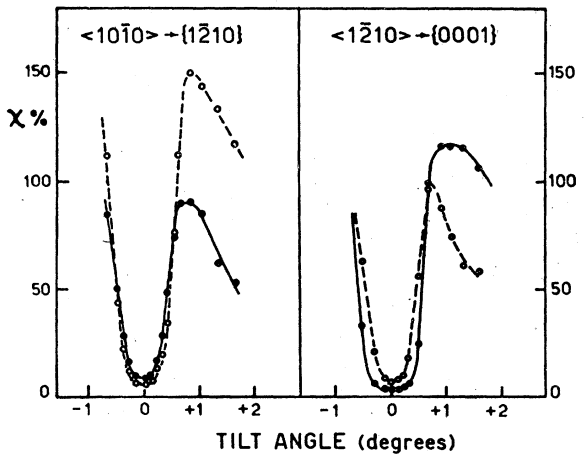

FIG. 8. Experimental yields for two axial-to-planar channeling transitions, as indicated in the upper part of the figure. Full and open circles refer to the yields from Al and O atoms, respectively.

the distance A-B in the previous figures. Numbers proportional to planar atomic densities are also shown. Figure 9(b) corresponds to the real lattice, with O-O nearest-plane distance equal to that of the Al-O planes. Figure 9(a) corresponds to equispaced O planes, following with a spacing equal to $\frac{1}{2}AB$. Figure 9(c) corresponds to O planes following alternatively with $AB/4$ and $\frac{3}{4}AB$ spacing, as the {111} planes in Si, and Figure 9 d corresponds

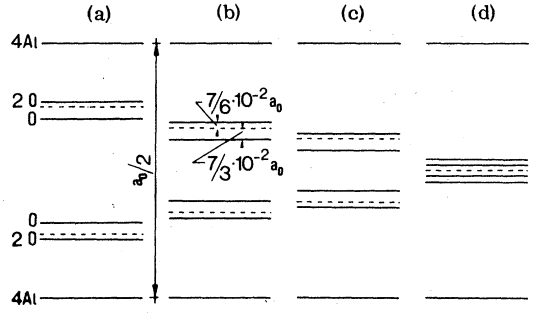

FIG. 9. Variation of the {1$\bar{2}$10} interplanar spacing in our computer experiments. To every plane is associated a coefficient proportional to the atomic density. The dashed lines refer to the center of mass of the O atoms. Case (b) corresponds to the actual situation ($d_{O\text{-}O} = d_{Al\text{-}O} = \frac{1}{3} d_{Al\text{-}Al}$). Case (a) corresponds to equispaced O planes ($d_{O\text{-}O} = \frac{1}{2} d_{Al\text{-}Al}$, $d_{Al\text{-}O} = \frac{1}{4} d_{Al\text{-}Al}$). Case (c) corresponds to O planes following in the O sublattice in the same sequence as the {111} planes in the Si lattice ($d_{O\text{-}O} = \frac{1}{4} d_{Al\text{-}Al}$, $d_{Al\text{-}O} = \frac{3}{8} d_{Al\text{-}Al}$, which makes the distance between two farthest O planes $2d_{Al\text{-}O} = \frac{3}{4} d_{Al\text{-}Al}$). Case (d) corresponds to making the two nearest O planes coincide ($d_{O\text{-}O} = 0$, $d_{Al\text{-}O} = \frac{1}{2} d_{Al\text{-}Al}$).

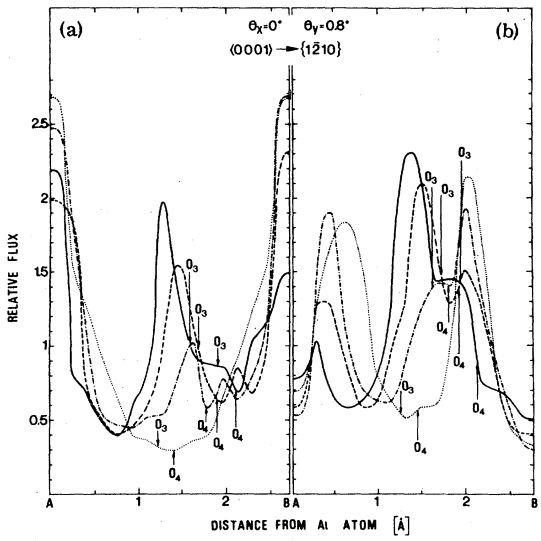

FIG. 10. Computed flux as in Fig. 6(b) and 7 at the ⟨0001⟩→{1$\bar{2}$10} transition ($\Theta_y = 0.8°$). Left-hand side (a) refers to the O sublattice alone, right-hand side (b) to the Al_2O_3 lattice. Continuous, dashed, dot-dash, and dotted lines refer in order to the structures shown in Fig. 9(a), 9(b), 9(c), 9(d). O_3 and O_4 have the same meaning as in Fig. 6 and are given on each curve.

to making the O planes coincide halfway between the Al planes.

Figure 10 shows the flux distribution along the A-B line at the transition (0.8° from the ⟨0001⟩ axis) both for the isolated O sublattice [left-hand side, (a)] and the Al_2O_3 lattice [right-hand side, (b)]. The sequence continuous, dashed, dot-dash, and dotted curve in Fig. 10 corresponds to decreasing spacing between the two closer oxygen planes as shown in Fig. 9(a)–9(d). O_3 and O_4 have the same meaning as in Figs. 6 and 7, and are shown on each flux curve. Figure 10(a) clearly shows that the flux inside the two O planes decreases with decreasing spacing. On the other hand, the farther apart the two O planes are, the lower is the fractional flux thrown on the O atoms near the transition. Therefore, the two effects compensate, at least in the range of interplanar spacings considered, remaining as an average around 80% near the O atoms (see curve b of Fig. 5 at 0.8°), except for the limiting case of overlapping O planes (dotted curve) for which the flux on the oxygen atoms is much less, around 30%. The introduction of the Al sublattice [Fig. 10(b)] shows on the other hand that the interplanar spacing effectively occurring in nature represents an optimum condition. In fact by increasing the relative distance between the two O planes, we reduce the Al-O spacing, decreasing the flux on the other side

of the O plane. This reduces strongly the contribution to the yield at the transition due to pushing of channeled particles from Al atoms against the O atoms. As a result the average yield around the O atoms is not much higher than 100% in the case of the continuous curve of Fig. 10(b), corresponding to the largest spacing between O planes. In conclusion the real experimental situation in which aluminum and oxygen planes follow at equal distances corresponds to an optimum condition of having much higher than 100% shoulder at the axial-to-planar channeling transition. By reducing the O-O interplanar spacing the flux inside them is reduced too much and the same happens by reducing the Al -O interplanar spacing.

C. Single trajectories

Last, we tried to display the characteristic features of single trajectories at the transition. Figure 11 shows two cases, starting between the Al-O and the O-O planes, respectively. Among the different trajectories we have chosen two for each case, one of which remains channeled up to the examined depth, while the other is dechanneled. The figure shows that all these trajectories correspond to a period of oscillation equal to the distance d_s between two subsequent strings of a plane. In particular this is clearly displayed in the case of the channeled trajectory between the Al and O planes, but looking carefully one sees that the case is the same for every trajectory, at least as far as the ion can be considered to be channeled. Even when the trajectory becomes unstable one sees that a stronger impulse which varies the curvature of the trajectory is received by the incident particle in correspondence of a row. The latter feature can be connected with the recent suggestion by Mukherjee,[19] according to which the transverse-plane focussing discussed by Barrett[20] can be interpreted in terms of resonant oscillations. The part of our dechanneled trajectories preceding the large-angle scattering event resembles the two-step path with which Mukherjee replaces the transverse-plane focussed trajectory. Our channeled trajectory of Fig. 11 starting between the O-O plane can be considered an intermediate case between a regularly oscillating and a dechanneled one.

We can conclude that the trajectories shown in Fig. 11 correspond to the first-order resonance predicted by Kumakhov and Wedell [see Eq. (14) of Ref. 9]. In this case using their notation one has

$$\omega = 2\pi v_\perp / d_s \,, \tag{1a}$$

and taking into account that $\omega = 2\pi v_\perp / \lambda_\perp$ one

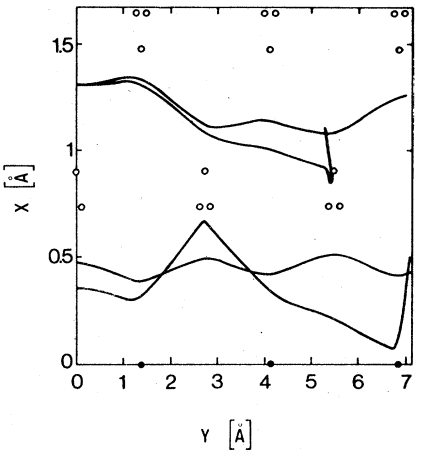

FIG. 11. Projection upon $\{1\bar{2}10\}$ of paths of ions moving with an angle $\Theta_y = 0.8°$ ($\Theta_x = 0°$) with respect to the $\langle 0001 \rangle$ axis. Notice the different scales along the X and Y axes. The depth travelled along $\langle 0001 \rangle$ is 500 Å. Full circles denote Al atoms, open ones O atoms.

gets

$$\lambda_\perp = d_s \,. \tag{1b}$$

Higher-order resonances, of the kind observed in transmission by Bulgakov and Shul'ga,[7] are expected to occur at higher angles, of the order of 3, 5, etc., times 0.8^0, even though this must be considered as a rough approximation. In fact ω depends somewhat on the transverse energy because the equation of motion is not purely harmonic [see Eq. (8a) of Ref. 9].

Since in our experiments no attention was paid to controlling accurately if any backscattered intensity fluctuation above the planar level occurs at these angles, we did not pursue any further computer analysis in this direction.

VI. CONCLUSIONS

The present work shows both experimentally and by computer calculations that the axial-to-planar channeling transition cannot be described by oversimplified models, giving relatively simple relationships, as it happens for the usual parameters characterizing channeling (such as critical angles, minimum yields, etc.). The transition depends strongly on the crystal structure and scattering power of rows and planes. In particular, in diatomic compounds completely different situations may arise and the same crystal may display shoulders higher or lower than random level in close

connection with the interplanar spacing among the various sublattices. The use of a computer appears to be of great value for a clear understanding of the experimental results and it makes possible to simulate situations which do not occur in nature but can give indications of how to disentangle the physical phenomena involved.

ACKNOWLEDGMENTS

The authors wish to thank Dr. M. Servidori for determining the orientation of the α-Al_2O_3 crystals by x rays. The experimental part of this work was performed at Laboratori Nazionali di Legnaro, Italy.

---

*Also Istituto Chimico, Facoltà di Ingegneria, Università di Bologna, Bologna, Italy.

[1]G. Della Mea, A. V. Drigo, S. Lo Russo, P. Mazzoldi, G. G. Bentini, A. Desalvo, and R. Rosa, Phys. Rev. B 7, 4029 (1973).
[2]U. Bill, R. Sizmann, C. Varelas, and K. E. Rehm, Radiat. Eff. 27, 59 (1975).
[3]J. A. Davies, J. Denhartog, and J. L. Whitton, Phys. Rev. 165, 345 (1968).
[4]J. U. Andersen, J. A. Davies, K. O. Nielsen, and S. L. Andersen, Nucl. Instrum. Methods 38, 210 (1965).
[5]H. Tittel, C. Varelas, and F. Bell, Phys. Lett. A 60, 151 (1977).
[6]G. Dearnaley, I. V. Mitchell, R. S. Nelson, B. W. Farmery, and M. W. Thompson, Philos. Mag. 18, 985 (1968).
[7]Yu. V. Bulgakov and V. I. Shul'ga, Fiz. Tverd. Tela 17, 353 (1975) [Sov. Phys. Solid State 17, 224 (1975)]; Radiat. Eff. 28, 15 (1976).
[8]A. Desalvo and R. Rosa, Phys. Rev. B 9, 4605 (1974).
[9]M. A. Kumakhov and R. Wedell, Phys. Status Solidi B 76, 119 (1976).
[10]G. Della Mea, A. V. Drigo, S. Lo Russo, P. Mazzoldi, S. Yamaguchi, G. G. Bentini, A. Desalvo, and R. Rosa, *Atomic Collisions in Solids*, edited by S. Datz, B. R. Appleton, and C. D. Moak (Plenum, New York, 1975). Vol. 2, p. 791.
[11]G. Della Mea, A. V. Drigo, S. Lo Russo, P. Mazzoldi, S. Yamaguchi, G. G. Bentini, A. Desalvo, and R. Rosa, Phys. Rev. B 10, 1836 (1974).
[12]A. Carnera, G. Della Mea, A. V. Drigo, S. Lo Russo, P. Mazzoldi, G. G. Bentini, A. Desalvo, and R. Rosa, Proceedings of the Seventh International Conference on Atomic Collisions in Solids, Moscow, 1977 (unpublished).
[13]A. V. Drigo, S. Lo Russo, P. Mazzoldi, P. D. Goode, and N. E. W. Hartley, Radiat. Eff. 33, 161 (1977).
[14]A. Carnera, G. Della Mea, A. V. Drigo, S. Lo Russo, P. Mazzoldi, and N. E. W. Hartley, Radiat. Eff. 14, 201 (1978).
[15]J. H. Barrett, Phys. Rev. 166, 219 (1968).
[16]V. A. Ryabov, Phys. Status Solidi B 49, 467 (1972).
[17]R. Hellborg, Phys. Scripta 3, 279 (1971).
[18]D. V. Morgan and D. P. Jackson, Radiat. Eff. 29, 99 (1976).
[19]S. D. Mukherjee, in Ref. 12.
[20]J. H. Barrett, Phys. Rev. Lett. 31, 1542 (1973).